

Double-Layered Boundary Extraction Method with Accurate Dielectric Constant Estimation for UWB Internal Imaging Radar

Shouhei Kidera

Graduate School of Informatics and Engineering,
University of Electro-Communications, Japan
Email: kidera@ee.uec.ac.jp

Abstract—A microwave ultra-wideband (UWB) radar system has an advantage for high range resolution and penetrating ability in dielectric object, and is promising for the applications, such as non-destructive testing for aging road or bridge and non-invasive human body inspection. We have already developed an accurate and high-resolution target boundary extraction method as range points migration (RPM) method, which are the advanced algorithm of spatial domain interferometer being applicable to non-point wise target shape. In this paper, we introduce the novel method for extracting double-layered dielectric object by using RPM based approach, where a dielectric constant of surrounding medium is simultaneously determined. The results obtained from the experiment assuming concrete objects, demonstrate the effectiveness of our proposed method.

Index Terms—UWB radars, Dielectric constant estimation, Boundary extraction, Non-destructive testing, Range points migration (RPM) method, Inverse scattering

I. INTRODUCTION

There are intensive demands for an innovative imaging techniques aiming at an object embedded in dielectric medium, which is promising for non-invasive medical screening of human body or and monitoring sensor for aging road or bridge. Microwave UWB (Ultra Wideband) radar system becomes one of the most promising technologies with the advantage for higher range resolution and ability to penetrate dielectric objects. In the inverse scattering issue, various reconstruction algorithms for target buried in the dielectric medium have been developed, for example the time-reversal method [1] and the space-time beamforming method [2]. However, these methods are based on the delay-and-sum approach assuming point-wise target, and then, the accuracy or spatial resolution is often insufficient for not point-wise target and its computational burden becomes enormous for extension to the 3-D problem.

For a promising approach of the above problem, we have already proposed a high-speed and accurate internal imaging method [4], based on the extended principle of the RPM method [3]. However, this study also revealed the problem that the imaging accuracy seriously depends on the assumed dielectric constant, which should be estimated in the practical application. There are various methods for reconstructing both the real and imaginary parts of permittivity, so called inverse scattering analysis, such as the numerical or analytical solution for domain integral equations [5]. However, this type of

approaches requires the multidimensional optimization for the discretized space of the region of interesting (ROI), and the number of variable dimensions must be severely constrained to avoid sluggish convergence in the optimization process. While other approaches such as in [6] require less computational burden by using the geometric optics (GO) approximation, they assume only a simple and known structure of the dielectric medium, such as a cuboid, and need to accurately estimate a dielectric boundary and its normal vector, beforehand.

For this background, this paper introduces the imaging method of simultaneously obtaining an accurate internal image and estimating a dielectric constant of surrounding medium. This method employs the range points migration (RPM) [3] and the Envelope interpolation methods [7] to correctly reconstruct dielectric boundary points and their normal vectors at a stage prior to internal imaging. The actual time delay of the propagating through the dielectric medium can then be accurately estimated from the recorded transmissive data. Moreover, in the case of a dielectric medium with a wavelength scale, the transmissive waveform differs from the transmitted waveform, and it reduces the accuracy of the measurement of the time delay. Then, our method has the additional property of compensating for the error caused by the above waveform deformation by iteratively generating the observation data using a finite-difference time domain (FDTD) method. The results from both numerical and experimental simulations demonstrate that our proposed method simultaneously determines both dielectric constant and each boundary of layered dielectric object, without *a priori* information of shape of each layer.

II. SYSTEM MODEL

Figure 1 shows the system model. It assumes that a target and homogeneous dielectric medium have an arbitrary shape with a clear boundary. The internal target can be located anywhere within the dielectric medium, which also has arbitrary position. A mono-cycle pulse is used as the transmitting signal, the center wavelength of which is defines as λ . The propagation speed c of the radio wave in air is a known constant. Two omni-directional antennas scan along the circle with a center r_c and radius R_c that completely surrounds a dielectric object as shown in Fig. 1. One transmitting and receiving

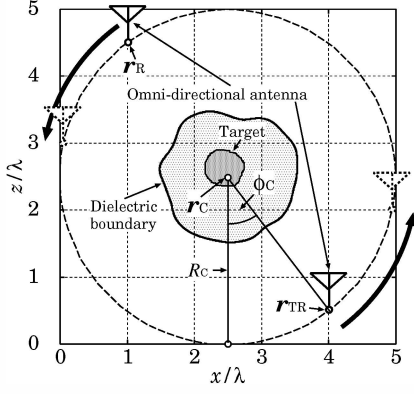


Fig. 1. System model.

antenna is located at $\mathbf{r}_{\text{TR}} = (X_{\text{tr}}, Z_{\text{tr}})$, and an antenna playing only a receiving role is located at $\mathbf{r}_{\text{R}} = (X_{\text{r}}, Z_{\text{r}})$, where $\mathbf{r}_{\text{c}} = (\mathbf{r}_{\text{TR}} + \mathbf{r}_{\text{R}}) / 2$ holds. $S_{\text{TR}}(\mathbf{r}_{\text{TR}}, R)$ and $S_{\text{R}}(\mathbf{r}_{\text{R}}, R)$ are defined as the outputs of the Wiener filter at antenna positions \mathbf{r}_{TR} and \mathbf{r}_{R} , respectively, where $R = ct/2$ is expressed by time t .

III. DIELECTRIC CONSTANT ESTIMATION WITH EXTENDED RPM METHOD

As mentioned in Sec. 1, while there are various studies for dielectric constant estimation, there are some limitations or inappropriate features for the problem presented in this study. To overcome the above difficulties, this paper introduces a novel non-parametric dielectric constant estimation method that is suitable for a clear dielectric boundary. The methodology of this method is detailed as follows.

A. Dielectric Boundary Extraction with RPM

First, this method employs the dielectric boundary points produced by the original RPM method, which achieves extremely accurate imaging employing the extracted range points defined as $\mathbf{q}_{\text{tr},i} = (X_{\text{tr},i}, Z_{\text{tr},i}, R_{\text{tr},i})$, ($i = 1, \dots, N_{\text{tr}}$). These components are extracted from the local maxima $S_{\text{TR}}(\mathbf{r}_{\text{TR}}, R)$, and N_{tr} denotes the total number of the range points. The RPM method then directly converts these range points to the target boundary points as $\mathbf{r}_i = (x_i, z_i)$, ($i = 1, \dots, N_{\text{tr}}$), where one-to-one correspondence is satisfied [3]. Furthermore, in order to avoid a sparse distribution of these points, the Envelope interpolation scheme is adopted as similar in [7]. A set of these target points is defined as \mathcal{T}_{rpm} . Note that the normal vector at each target boundary point is calculated without a derivative operation as $\mathbf{e}_{n,i} = (X_{\text{tr},i} - x_i, Z_{\text{tr},i} - z_i) / R_{\text{tr},i}$.

B. Dielectric Constant Estimation with Transmissive Data

For calculating the propagation path, the incident and exit points ($\hat{\mathbf{r}}_{\text{I}}(\epsilon_t), \hat{\mathbf{r}}_{\text{E}}(\epsilon_t)$) on the dielectric boundary are deter-

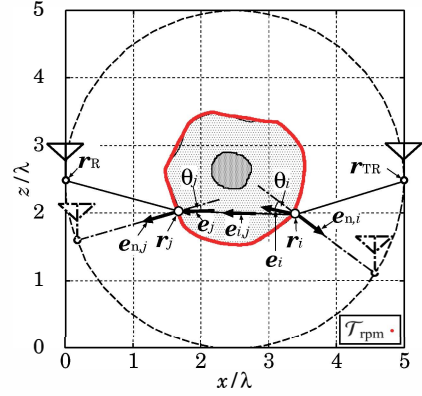


Fig. 2. Spatial relationship among the incident, exit boundary points and antenna locations, and obtained dielectric boundary points as \mathcal{T}_{rpm} .

mined by the Snell's law:

$$(\hat{\mathbf{r}}_{\text{I}}(\epsilon_t), \hat{\mathbf{r}}_{\text{E}}(\epsilon_t)) = \arg \min_{(\mathbf{r}_i, \mathbf{r}_j) \in \mathcal{T}_{\text{rpm}}^2} \left\{ \|e_i(\epsilon_t) - e_{i,j}\|^2 + \|e_j(\epsilon_t) - e_{i,j}\|^2 \right\}, \quad (1)$$

where ϵ_t is a relative permittivity of dielectric medium, $e_i(\epsilon_t) = \mathbf{R}_o(\theta_i(\epsilon_t))(-e_{n,i})$, $e_j(\epsilon_t) = \mathbf{R}_o(\theta_j(\epsilon_t))(-e_{n,j})$ and $e_{i,j} = (\mathbf{r}_i - \mathbf{r}_j) / \|\mathbf{r}_i - \mathbf{r}_j\|$. $\mathbf{R}_o(\theta)$ is a rotation matrix in the counterclockwise direction, and $\theta_i(\epsilon_t)$ and $\theta_j(\epsilon_t)$ denote the refraction angles calculated by Snell's law. Figure 2 shows the estimated dielectric boundary produced by Envelope, and spatial relationship among the incident, exit boundary points and the antenna locations. Then, the estimated dielectric medium for each range point is then determined by

$$\epsilon_t^{\text{init}}(\mathbf{q}_{r,i}) = \arg \min_{\epsilon_t} |R(\epsilon_t : X_{r,i}, Z_{r,i}) - R_{r,i}|, \quad (2)$$

where $R(\epsilon_t : X_{r,i}, Z_{r,i})$ is the estimated propagation delay obtained by $(\hat{\mathbf{r}}_{\text{I}}(\epsilon_t), \hat{\mathbf{r}}_{\text{E}}(\epsilon_t))$ and $\epsilon_t, \mathbf{q}_{r,i} = (X_{r,i}, Z_{r,i}, R_{r,i})$, ($i = 1, \dots, N_{\text{r}}$) are extracted from the maxima of $S_{\text{R}}(X, Z, R)$. Using all the transmissive range points, the initial relative permittivity $\hat{\epsilon}_t^{\text{init}}$ is estimated as

$$\hat{\epsilon}_t^{\text{init}} = \frac{\sum_{\mathbf{q}_{r,i} \in Q} S_{\text{R}}(\mathbf{q}_{r,i}) \epsilon_t^{\text{init}}(\mathbf{q}_{r,i})}{\sum_{\mathbf{q}_{r,i} \in Q} S_{\text{R}}(\mathbf{q}_{r,i})}, \quad (3)$$

where Q denotes the set of range point \mathbf{q}_{r} .

Note that the above procedure is basically derived from the geometrical optics approximation, where the frequency characteristic in transmissive phenomena is not taken into consideration. However, in the case of a dielectric medium of wavelength scale, this frequency characteristic is not negligible and it causes the waveform deformation of transmissive data, which reduces the accuracy of the relative permittivity estimation, owing to the inaccuracy of the range points.

C. Waveform Correction with FDTD Method

To mitigate this type of accuracy degradation, we introduce an iterative procedure to compensate the range point error

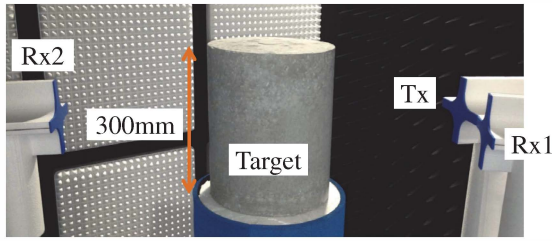


Fig. 3. Setup for the experiment (upper) and setup for obtaining actual dielectric constant of cement object(lower).

caused by waveform deformation using an FDTD. Specifically, we regenerate the transmissive data as $\tilde{S}_R(\mathbf{r}_R, R)$ using the FDTD, where the dielectric boundary points as \mathcal{T}_{rpm} and the estimated relative permittivity as $\hat{\epsilon}_t^{\text{init}}$ are employed for FDTD data generation. Next, the range correction $\Delta R(\mathbf{q}_{r,i})$ at each range point $\mathbf{q}_{r,i}$ is determined from the peak shift of the correlation function between the measured $S_R(\mathbf{r}_R, R)$ and the regenerated transmissive data $\tilde{S}_R(\mathbf{r}_R, R)$. The estimated relative permittivity $\epsilon_t(\mathbf{q}_{r,i})$ for each range point is then corrected:

$$\epsilon_t(\mathbf{q}_{r,i}) = \left\{ \sqrt{\hat{\epsilon}_t^{\text{init}}} + \frac{\Delta R(\mathbf{q}_{r,i})}{L_\epsilon(\mathbf{q}_{r,i})} \right\}^2, \quad (4)$$

where $L_\epsilon(\mathbf{q}_{r,i}) = \sqrt{\hat{\epsilon}_t^{\text{init}}} \|\hat{\mathbf{r}}_I(\epsilon_t) - \hat{\mathbf{r}}_E(\epsilon_t)\|$ is the estimated propagation distance in the dielectric medium for $\mathbf{q}_{r,i}$. Finally, the relative permittivity $\hat{\epsilon}_t$ is updated as

$$\hat{\epsilon}_t = \frac{\sum_{\mathbf{q}_{r,i} \in Q} S_R(\mathbf{q}_{r,i}) \epsilon_t(\mathbf{q}_{r,i})}{\sum_{\mathbf{q}_{r,i} \in Q} S_R(\mathbf{q}_{r,i})}, \quad (5)$$

IV. PERFORMANCE EVALUATION IN EXPERIMENT

This section describes the experimental validation of the method previously mentioned. Figure 3 illustrates the experimental setup. The cylindrical aluminum (internal object) is buried in the cylindrical cement (dielectric object), and they are both 250 mm high. The radii of the cement and aluminum objects are 139 mm and 25 mm, respectively. The circular scanning model described in Sec. II is equivalently accomplished by rotating the dielectric object along the center \mathbf{r}_C , fixing the location of the antennas \mathbf{r}_{TR} , \mathbf{r}_{R1} and \mathbf{r}_{R2} . Here, S_{TR} and S_R are regarded as the received signals at the antennas located at \mathbf{r}_{R1} and \mathbf{r}_{R2} , respectively, where the transmitting antenna is \mathbf{r}_{TR} . The target rotation center is set to $\mathbf{r}_C = (400\text{mm}, 400\text{mm})$, and the distance from the antenna, namely, R_C is set to 400 mm. The received signal is obtained using a VNA (Vector Network Analyzer), where the frequency is swept from 1000 MHz to 3000 MHz at 10 MHz intervals. Vertical linear polarization is assumed in both the transmitting and receiving antennae, which are dipole antennae in the vertical direction. S_{TR}, S_R are obtained by applying the inverse discrete Fourier transform to these frequency data. The effective bandwidth is around 2.0 GHz, namely, the range resolution is around 75 mm. The center frequency is also

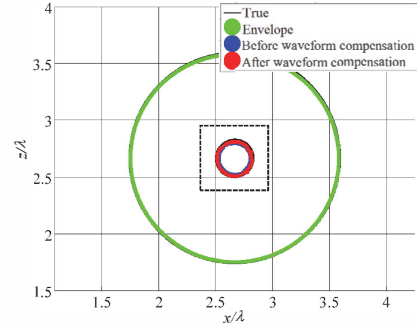
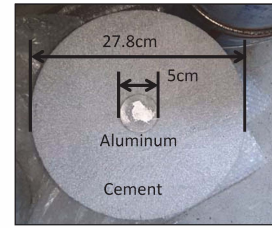


Fig. 4. Actual and reconstructed outer and inner dielectric boundary (upper: actual view, upper: reconstructed).

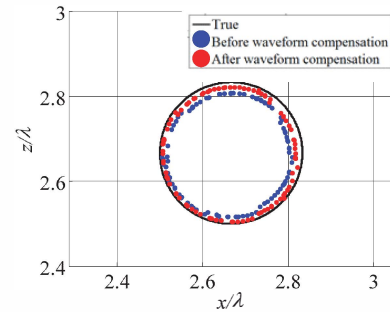


Fig. 5. Enlarged view of Fig. 4 focusing on the buried object area.

2.0 GHz (center wavelength : 150 mm). The actual dielectric constant of the dielectric object (cement) is measured as 9.07 by assessing the propagation delay when observing a cement object with a cuboid shape.

The average SNR for reflection signals from outer and inner boundaries received at \mathbf{r}_{R2} are 51 dB and 35 dB, respectively. Also, the average SNR for transmissive signals received at \mathbf{r}_{R1} is 43 dB. Note that, the SNR is defined as the ratio of the peak instantaneous signal power to average noise power after applying a matched filter. This is the most strict definition, considering both time and frequency localities of a received signal, and each SNR is estimated relatively higher compared with a general SNR definition. The weighted average dielectric constants before and after waveform compensation are 8.52 and 8.80, and the relative errors are 6 % and 3% respectively. This shows that the proposed method accomplishes highly accurate dielectric constant estimation without knowledge of the shape of the dielectric media using real data. Furthermore, Fig. 4 illustrates the actual and estimated dielectric and buried target boundary points, which are reconstructed employing the

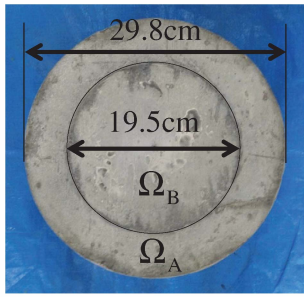


Fig. 6. Concrete target with double-layered structure.

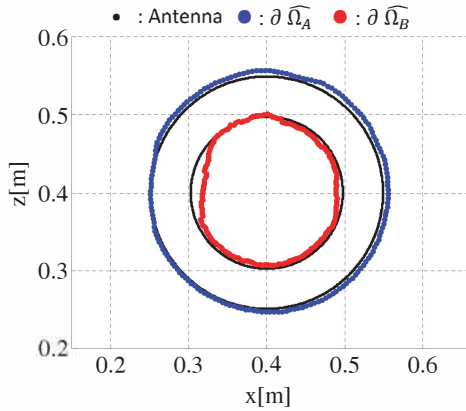


Fig. 7. Estimated dielectric boundaries for Ω_A and Ω_B using the proposed method in the experiment.

method in [4] using \mathbf{R}_{R2}^D and \mathbf{R}_{R2}^T , respectively, before and after waveform compensation. Figure 5 shows an enlarged view of Fig. 4 focusing on the internal imaging area. This figure denotes that the FDTD based waveform compensation enhances the accuracy of inner object imaging. The mean error for dielectric constant estimation before and after waveform compensations are $1.98 \times 10^{-2}\lambda$ and $0.97 \times 10^{-2}\lambda$, respectively.

A. Extension to Double-Layered Dielectric Object Case

Furthermore, the case of double layered medium (both medium have lower conductivity) is investigated as follows. Our method is basically extended to the multiple layered medium by introducing the boundary extraction method as RPM or Envelope method for each layer. In this experiment, another case that a cylindrical mortal mix Ω_B is buried in the cylindrical cement Ω_A , and both cylinders are 300mm high, is investigated as follows. The radii of the mortal and cement mediums are 298 mm and 195 mm, respectively. The actual dielectric constants of the dielectric object (cement and mortal) were measured by averaging the propagation delays observed from 50 different angles, assuming a cylindrical dielectric object fabricated from each material. In this way, the dielectric constants of the cement and mortal objects are measured as approximately 10.9 and 9.7, respectively, which are regarded as the actual values in this experiment. Here, the

average S/Ns of $S_1(X, Z, R)$ and $S_2(X, Z, R)$ are 42 dB, 34 dB, respectively. In addition, to suppress the range sidelobe caused by relatively narrower fractional bandwidth of the transmitted signal compared with that assumed in numerical simulation, the Capon filter is used for range point extraction. In this case, the estimated dielectric constants are estimated as $\hat{\epsilon}_A = 10.68$ (relative error of 2.5%) and $\hat{\epsilon}_B = 9.02$ (relative error of 7%), respectively. Figure 7 shows each reconstructed image of the double layered dielectric media, as $\partial\hat{\Omega}_A$ and $\partial\hat{\Omega}_B$, respectively, where the estimated dielectric constants are used for the extended Envelope method. The RMSEs of outer and inner boundary are about 6.5 mm ($4.3 \times 10^{-2}\lambda$) and 7.7 mm ($5.1 \times 10^{-2}\lambda$), respectively. This result confirms that our proposed method enables highly accurate boundary extraction in realistic scenarios; indeed, the accuracy is on the order of 1/100 of the transmitting wavelength, which is sufficient for practical applications.

V. CONCLUSION

This paper proposed an accurate estimation method for dielectric constants and boundary shapes of double-layered dielectric object. As a notable feature of this method, it is applicable to arbitrary target shape, and offers an accurate estimation for both dielectric constant and boundary extraction without *a priori* knowledge of shape of each boundary. In addition, this method exploits a unique characteristic of the RPM method, which accurately offers not only boundary points but also normal vector on them. This feature enables us to determine the possible propagation path penetrating into double-layered dielectric medium using Snell's law. The experimental investigation revealed that our proposed method provided a considerably accurate dielectric constant estimation, which contributes each boundary extraction with the accuracy at the order of 1/100 transmitting center wavelength.

REFERENCES

- [1] P. Kosmas, and C. M. Rappaport, "A Matched-Filter FDTD-Based Time Reversal Approach for Microwave Breast Cancer Detection," *IEEE Trans. Antennas Propagat.*, vol. 54, no. 4, pp. 1257–1264, Apr., 2006.
- [2] X. Li, E. J. Bond, B. D. Van Veen, and S. C. Hagness, "An overview of Ultra-Wideband Microwave Imaging via Space-Time Beamforming for Early-Stage Breast-Cancer Detection," *IEEE Antennas Propagat. Mag.*, vol. 47, no. 2, pp. 19–34, Feb., 2005.
- [3] S. Kidera, T. Sakamoto, and T. Sato, "Accurate UWB Radar 3-D Imaging Algorithm for Complex Boundary without Range Points Connections," *IEEE Trans. Geosci. Remote Sens.*, vol. 48, no. 48, pp. 1993–2004, Apr., 2010.
- [4] K. Akune, S. Kidera, and T. Kirimoto, "Accurate and Nonparametric Imaging Algorithm for Targets Buried in Dielectric Medium for UWB Radars," *IEICE Trans. Electronics*, vol. E95-C, no. 8, pp. 1389–1398, Aug., 2012.
- [5] R. Autieri, M. Urso, T. Isernia, and V. Pascazio, "Inverse Profiling via an Effective Linearized Scattering Model and MRF Regularization," *IEEE Trans. Geosci. & Remote Sens.*, vol. 8, no. 6, pp. 1021–1025, Nov., 2011.
- [6] J. Ren, Y. Zhang, T. Jiang, and W. Chen, "Estimation of Wall Parameters From Time-Delay-Only Through-Wall Radar Measurements," *IEEE Trans. Antennas Propagat.*, vol. 59, no. 11, pp. 4268–4278, Nov., 2011.
- [7] S. Kidera, T. Sakamoto, and T. Sato, "A Robust and Fast Imaging Algorithm with an Envelope of Circles for UWB Pulse Radars," *IEICE Trans. Commun.*, vol. E90-B, no. 7, pp. 1801–1809, Apr., 2007.